

Retro-Jet Experimental Study for Reusable Rockets in a Hypersonic Flow

Sungmin Lee and Gisu Park*[†]*

**Korea Advanced Institute of Science and Technology
Daehakro 291, Daejeon 34141, Republic of Korea
smtrust@kaist.ac.kr · gisu82@kaist.ac.kr*

[†]Corresponding author

Abstract

In this study, an experimental study on general flow characteristics was conducted using a retro-jet thruster module with helium cold gas as a basic study of the retro-propulsion on the entry vehicles. The qualitative measurement of the flow field was carried out using the schlieren photography, and the quantitative density measurement was conducted using the intrusive background oriented schlieren measurement. Retro-jet single plume thickness and oblique shock wave height were confirmed by measuring density variation according to position in the steady state of the retro-jet test flow field. Flow was established approximately 250 μ s after flow reached, which was confirmed by an increase rate of about 10% above the oblique shock wave height caused by retro-jet single plume thickness amplification. In addition, the retro-jet flow-interface distance and the nozzle thrust coefficient were measured to be 0.46 and 0.30, confirming that the test model base diameter did not significantly affect the flow-interface distance.

1. Introduction

At the same time as the space travel generation began, the use of the multistage launch vehicle for mission completion has been dominated. Although the multistage launch vehicle has been recognized as a reliable approach, research on alternatives has been continuously conducted due to the high launch costs consumed per time. As an ideal goal of alternative approaches, access to a single stage to orbit (SSTO) concept of completing and returning tasks without stage separation has been considered for decades. This technique is not achievable with current light weight materials as well as with chemical propulsion performance technology. Recently, attention has been focused on another alternative for reusable rocket to minimize the cost of access to space by various companies.^{2,35} These companies are developing designs ranging from fully reusable SSTO to more traditional expendable launch vehicles with reuse of high value components such as the first stage engine and/or its booster engines. Reusable technologies are divided into non-propulsive approaches and propulsive approaches. Non-propulsive approaches include aerodynamic decelerators including inflatable decelerators and parachutes, and terminal landing approaches including impact attenuators and mid-air recovery techniques.³⁰ In such technologies, supersonic and hypersonic inflatable decelerators and parachutes have problems such as parachute deployment problem and material limitation. As a result, research has been conducted as an alternative to effective deceleration in high speed flow through propulsive approaches.¹⁸

The study of reusable space booster and reusable rocket has been considered since the 1960s when space travel generation began. Horizontal landing and vertical landing have been considered in two ways to land safely on land. Vehicles with horizontal landing systems have the disadvantage that wings and undercarriages are required, while the relatively simple parachute method in vertical landing systems is only applicable to small landing vehicle such as re-entry capsules. The retro-propulsion method for an effective vertical landing system has been evaluated as reasonable and has received continuous attention from McDonnell Douglas DC-X.¹ The DC-X was studied by McDonnell Douglas from 1991 to 1996 as an unmanned reusable SSTO launch vehicle. Blue Origin² began developing a vertical take-off and landing (VTVL) spaceship called as New Shepard in 2005 and completed its first test flight in 2015. Since then, it has been successfully returned to earth with a soft landing for recovery and reuse until 2016. The Falcon9 series(Fig.1(a)), which has been developed since 2005 by SpaceX,³⁵ was first launched in 2010 and has been launched until 2018. Since then, a series of reusable rockets are being developed and launched using a launch vehicle called as Falcon Heavy. Research on retro-propulsion, one of the technologies required for VTVL, has been studied in various research institutes. Supersonic retro-propulsion flow forms an under-expanded jet flow in a supersonic and hypersonic

SHORT PAPER TITLE

free-stream simulated environment. The interaction between the retro-propulsion flow and the high speed free-stream has affected the aerodynamic characteristics around the launch vehicle.^{4,5,9,10,12,18,33,34,39,45} In the retro-propulsion single plume environment, the supersonic shear layer establishes along the outer jet boundary due to the large velocity gradients between the subsonic flow on the post of the bow shock and the opposing supersonic jet flow (Fig.1(b)).^{12,18} Since the 1960s when technology development programs for planetary exploration missions began, up until recently, research has been conducted at various research institutes including NASA. Daso et al⁹ investigated an active flow concept using counter flowing jets to significantly modify the external flow fields and strongly weaken or disperse the shock-waves of supersonic and hypersonic vehicles to reduce the aerothermal loads and wave drag. Berry et al.^{4,5} conducted an experimental study over the Mach number range from 2.4 to 4.6 in the Langley Research Center Unitary Plan Wind Tunnel Test Section2. In addition to the high spatial-density surface pressure measurements that were the main experimental objective, high speed schlieren video and internal pressures and temperatures measurements were conducted. The same test model was experimentally examined for Mach number 1.8 and 2.4 in the Ames Research Center 9x7-foot Supersonic Wind Tunnel by Rhode and Oberkamp.³³ Schauerhamer et al³⁴ conducted qualitative comparisons of the flow structure by comparing CFD to high-speed Schlieren images, and quantitative comparisons by comparing averaged surface pressure with pressure tap data from the Langley Research Center Unitary Plan Wind Tunnel Test Section2.

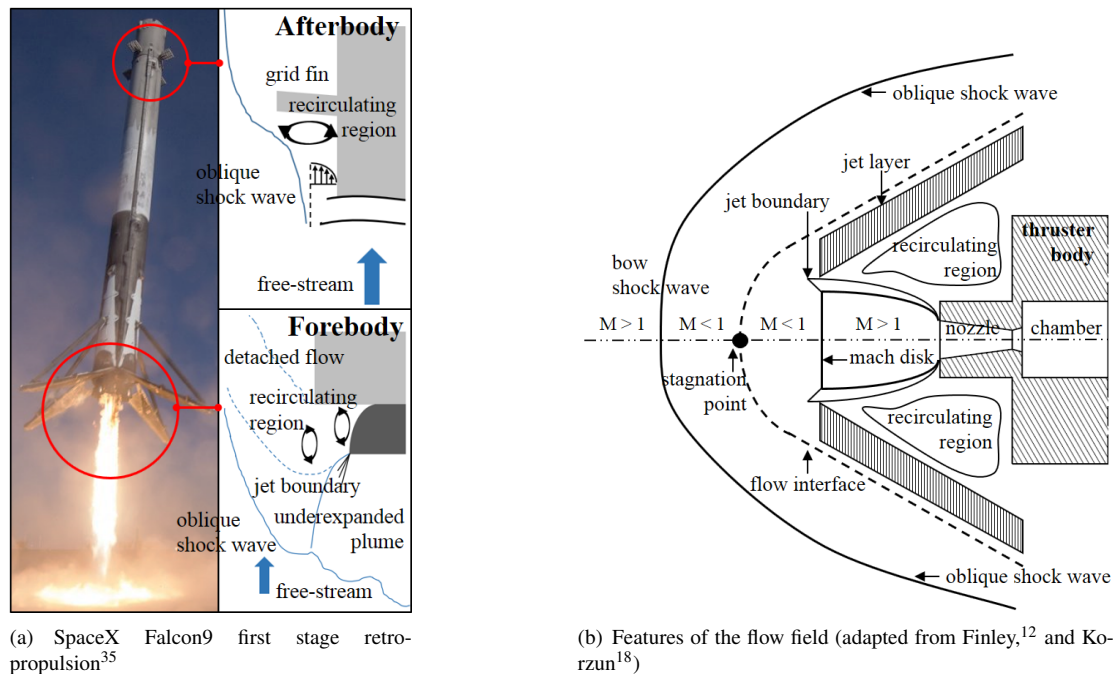


Figure 1: General flow field of the retro-propulsion study

The background oriented schlieren (BOS) is more advanced and provides additional quantitative information than other optical techniques such as shadowgraphy, schlieren photography, or interferometry. The BOS uses correlation techniques on a background dot image to quantitatively characterize compressible and thermal flows with good spatial and temporal resolution. The main advantages of this technique are that the experimental setup is simple and the robustness of correlation-based digital analysis, which is not only widely used, but also easy for users to use and adapt. A study on the BOS technique using particle image velocimetry (PIV) was started by Meier²⁸ to obtain more detailed quantitative flow field information (density field). The PIV technique has been applied to low speed and subsonic wind tunnels, and it was provided that the instantaneous velocity vector field in a planar cross section within the flow. The application of the BOS technique to the high speed flow environment has been actively conducted since the early 2000s.^{8,11,19,31,32,38,40-44} Raghunath et al³¹ tested a Mach 4 conical nozzle, with nozzle supply pressure of 2 MPa and nozzle supply temperature of 2000 K, respectively. The shock angles measured from the processed images were within 2% of the theoretical calculations and matched well with the results of the CFD simulations. Venkatakrishnan and Meier^{19,43} studied the application of the BOS technique to supersonic complex underexpanded jet flow. Pitot measurements made on an ideally expanded sonic jet were utilized for validation of BOS. This study showed that meaningful quantitative density data can be extracted by using minimal hardware with this methodology.

In this study, an experimental study on general flow characteristics was conducted using a retro-jet thruster mod-

ule with H_2 cold gas as a basic study of the retro-propulsion on the entry vehicles in an opposing hypersonic free-stream environment. The flow development of the retro-jet single plume and bow shock wave formed between retro-jet single plume and opposing free-stream. From the construction of the retro-jet thruster module, the qualitative measurement of the flow field was carried out by using the schlieren photography, and the quantitative density measurement was conducted by using the intrusive BOS measurement technique. By using the quantitatively measured data, we have demonstrated the applicability of the technique through quantitative analysis of the stability of bow shock wave and retro-jet plume height formed by the encounter of retro-jet single plume and opposing M6 free-stream.

2. Apparatus and tests

2.1 Test facility

The K1 shock tunnel used in this study is a reflected type impulse facility and consists of a shock tube, expansion nozzle, and test section composed of a driver tube and a driven tube. It is located in the Aerospace engineering department, Korea Advanced Institute of Science and Technology. Figure 2 shows a schematic of the K1 shock tunnel with retro-jet reservoir.

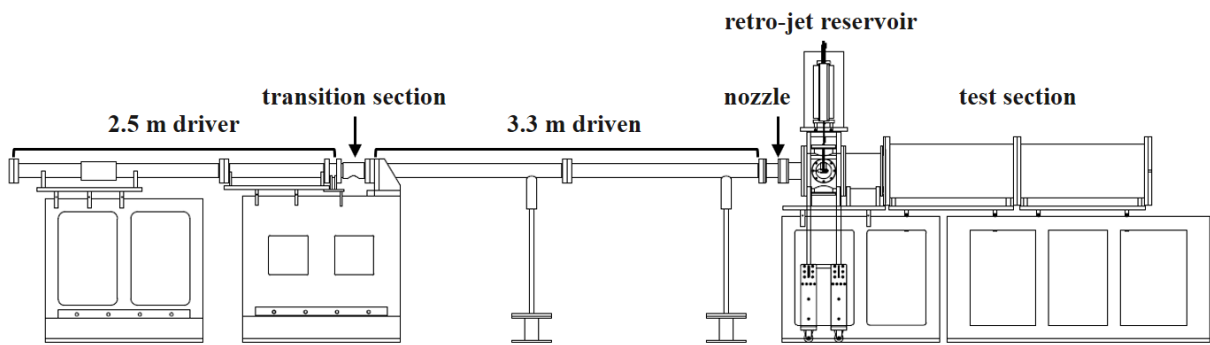


Figure 2: A schematic of the K1 shock tunnel²⁰

The K1 shock tunnel has a length of about 9 m including the test section, and the driver and driven tube lengths are 2.5 m and 3.3 m, respectively. Since 2010, the reliability of supersonic/hypersonic flow formation has been verified through various studies using shock tube and shock tunnel in two ways of this facility.^{6, 7, 14–17, 21–23, 29, 37} The flow condition used in this study is summarized as follows (Table 1).

2.2 Retro-jet thruster module

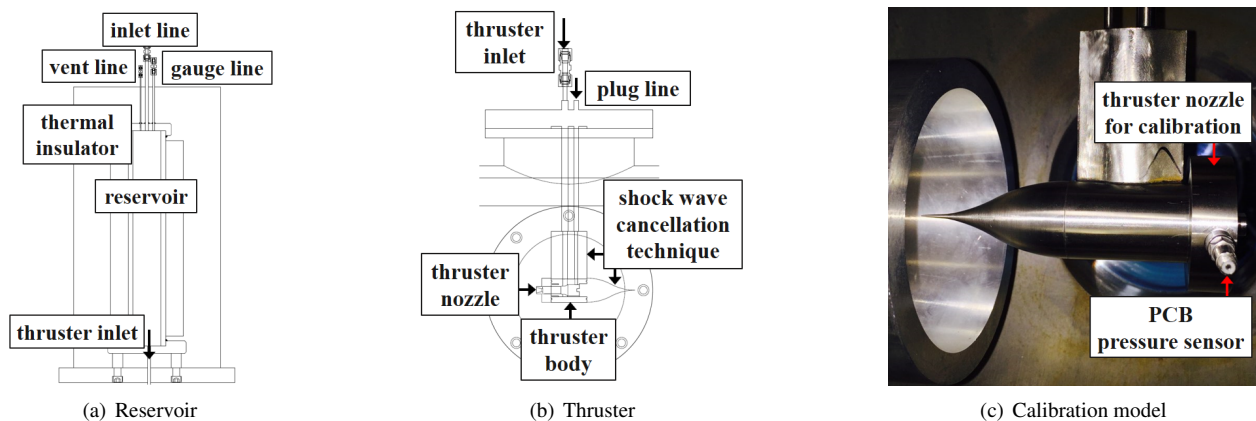


Figure 3: Retro-jet thruster module

A high pressure reservoir was additionally constructed to maximize the normal flow operation time of the retro-jet cold gas single plume (Fig. 3(a), (b)). Due to the limited space, a plug was inserted into the chamber for precise gas

SHORT PAPER TITLE

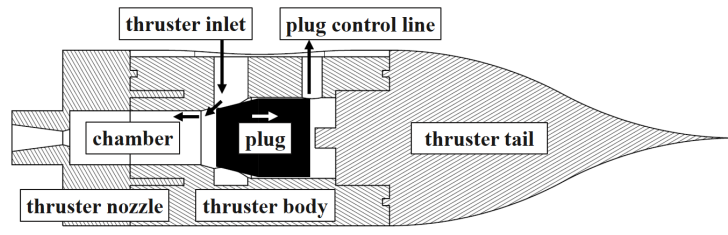


Figure 4: Retro-jet operation principle

injection control, and the plug was controlled using the pressure difference between the front and rear of the plug. Using this plug, it was possible to minimize the time required to develop the plume at the retro-jet thruster nozzle exit. In addition, the shock wave cancellation technique was applied to minimize the interference effect on free-stream flow in the side strut support and thruster tail part. The combustion chamber, nozzle throat, and nozzle exit of the retro-jet thruster used in this study are 8 mm, 2 mm, and 4 mm in diameter, respectively. The retro-jet thruster have a nozzle shape with an expansion ratio of 4(Fig.4). A stagnation pressure measurement was conducted at the end of the combustion chamber to confirm whether or not stagnation pressure was formed in the combustion chamber. The measurement uses a PCB piezoelectric pressure sensor with a fast response time of several microseconds (μ s) using an electrical signal generated by the piezoelectric effect to measure the flow characteristics in which steady flow established within a few milliseconds (ms)(Fig.3(c)). The retro-jet single plume flow conditions used in this study are summarized as follows(Table2).

Table 1: Free-stream flow condition

Property	Value
M_∞ [-]	6.0
H_0 [MJ/kg]	1.9
P_0 [bar]	19.1
T_0 [K]	1,919
P_∞ [kPa]	1.1
T_∞ [K]	231
ρ_∞ [kg/m ³]	0.016
u_∞ [m/s]	1,833

Table 2: Retro-jet single plume condition

Property	Value
M_∞ [-]	2.2
A_e/A_t [-]	4.0
P_0 [bar]	10
T_0 [K]	290
P_∞ [kPa]	93.5
T_∞ [K]	106
ρ_∞ [kg/m ³]	0.33
u_∞ [m/s]	1,335

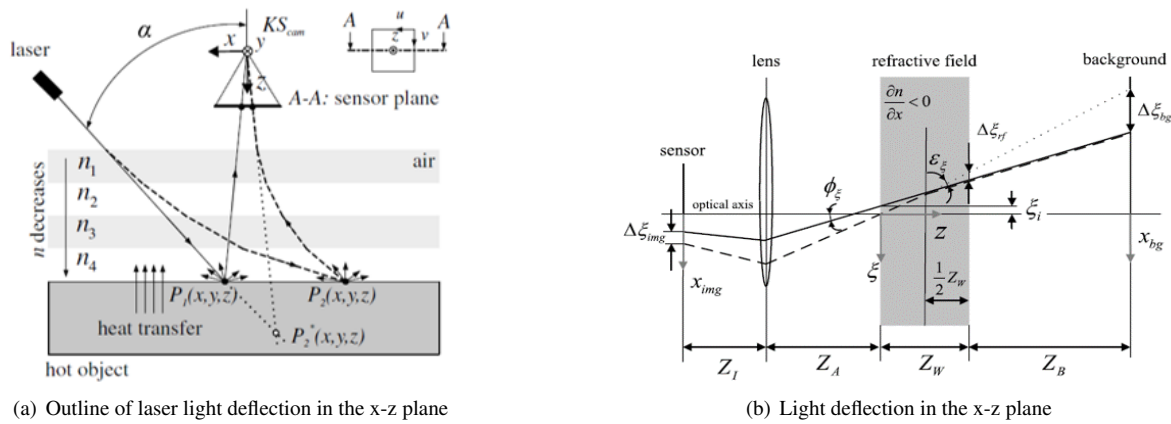
3. Background oriented schlieren

The background oriented schlieren (BOS) technique has evolved from visualization techniques such as shadowgraphy, schlieren photography, and interferometry to provide quantitative information. The BOS technique sensitively responds to the deflection angle(ϵ) of the ray in various refractive index fields. The relationship between density gradients and refractive index variations uses the Gladstone-Dale equations(Eq.1). Where n is the refractive index, ρ is the density(kg/m³), and $G(\lambda)$ is the Gladstone-Dale number(m³/kg)(Eq.2),

$$\frac{n-1}{\rho} = G(\lambda) \quad (1)$$

$$G(\lambda) = 2.2244 \times 10^{-4} \cdot \left(1 + \left(\frac{6.7132 \times 10^{-8}}{\lambda} \right)^2 \right) \quad (2)$$

A simplified schematic diagram of the relationship between the refractive index and the laser lightpath of an illumination is as follows(Fig.5(a)). When a homogeneous refractive index field is assumed, the laser lightpath has a beam that is not refracted. The actual position(P1(x,y,z)) of the hot object was represented by a solid line. A laser lightpath that is refracted due to an inhomogeneous refractive index field, which is formed from heat transferred from the object to the ambient air, was labeled as a dashed line. When assuming a homogeneous refractive index, P2*(x,y,z)

Figure 5: Light deflection in a refractive index field³

is seen as the actual position. It is different from the hot surface in location $P_2(x,y,z)$, where the dot was actually projected on.

In this way, the dot position on the optical sensor varies depending on the presence or absence of the variant refractive index field. According to Fermat's principle, the ray of light takes the path between two points which is the shortest distance in relation to the change of the path. To calculate the refractive index, the known light deflection, and a variational calculus problems can be formulated according to Fermat's principle. The path of light considered in this chapter is restricted to rays that have a component in the z direction (Eq.3,4).

$$\frac{d^2\xi}{dz^2} = \left[1 + \left(\frac{d\xi}{dz} \right)^2 + \left(\frac{d\zeta}{dz} \right)^2 \right] \frac{1}{n_0} \frac{\partial n}{\partial x} \quad (3)$$

$$\frac{d^2\zeta}{dz^2} = \left[1 + \left(\frac{d\xi}{dz} \right)^2 + \left(\frac{d\zeta}{dz} \right)^2 \right] \frac{1}{n_0} \frac{\partial n}{\partial y} \quad (4)$$

where ξ is the x -axis displacement, and η is the y -axis displacement. The second derivatives of the displacement of two directions are given as functions of the refractive index gradients $\frac{\partial n}{\partial x}$ and $\frac{\partial n}{\partial y}$. The applied coordinate systems are given in Fig.5(b).

In this study, the distortion of the x -axis and y -axis directions was recorded and standard computerized PIV methods are applied to extract the displacement field. Displacement data can be obtained from PIV measurement results, as well as density gradient distribution. The density gradient distribution is expressed by dividing the x -axis and y -axis directions as follows (Eq.5,6).

$$\frac{\partial \rho}{\partial x} = -\frac{K}{G(\lambda)} \cdot \Delta \xi \quad (5)$$

$$\frac{\partial \rho}{\partial y} = -\frac{K}{G(\lambda)} \cdot \Delta \zeta \quad (6)$$

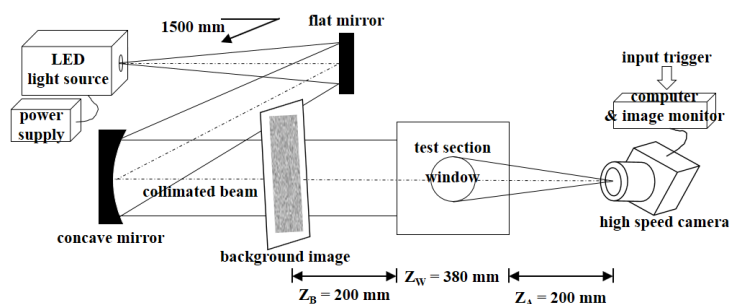


Figure 6: Schematic of BOS measurement

Density gradients from the PIV results obtained by using the background image as a particle pattern were integrated by grad2Surf Version 1.0 open source tool: surface reconstruction from Gradient Fields. The Gradient-to-Surface

SHORT PAPER TITLE

Toolbox, grad2Surf, is a Matlab toolbox for the reconstruction of a 2D surface from its gradient field. It is based on the reference.²⁴⁻²⁶ The BOS measurement method used in this study is as follows(Fig.6). A background dot image was added to schlieren photography which can measure the flow field qualitatively.

4. Results and discussion

4.1 Density measurement validation

A hemisphere of 30 mm diameter, and a cylinder model of 12 mm diameter and 90 mm width were used for validation of the BOS measurement. The hemisphere test confirmed the shock stand-off distance and density increase rate formed before and after the bow shock wave. Using the cylinder model, the density change from the model center line to the oblique shock wave in a region formed at the end of the model was measured and compared with the computational data. Computational study of the cylinder test for comparison with experimental results was performed through Fluent Ver. 16.1 in ANSYS package. The Pointwise Ver. 18.0 program was used to create the mesh file used for the analysis and to select the boundary conditions. The two-dimensional mesh generation for the axisymmetric calculation was same as the K1 shock tunnel apparatus used in this study. The surface of the model was assumed to be set as stationary wall with no slip and adiabatic condition, because the changes in surface temperature were usually quite small during the test time. The k-w SST turbulence model was used to predict the turbulent eddy viscosity and a parallel algorithm based on the domain decomposition strategy was used to reduce the large computation time associated with the flow calculations around the symmetric two-dimensional model. It is assumed that time marching proceeds until a steady-state solution is reached. Grid tests were performed on about 20,000, 40,000, 80,000 and 160,000 mesh cases. A grid with about 80,000 meshes was determined as the appropriate grid through the grid tests on model surface density, surface pressure coefficient, oblique and recompression shock waves shapes.

Figure 7(a),(b) show the background dot pattern imaged with the hemisphere model in the absence and presence of the flow respectively. The displacements calculated from these images were carried out by PIV program. An interrogation window of 8 by 8 pixels was found to be appropriate, and the step size was determined to be 2 by 2 pixels based on experience. Fig. 7(c) shows the displacements as a vector field, and Fig.7(d) shows the density field as a gray scaled contour image.

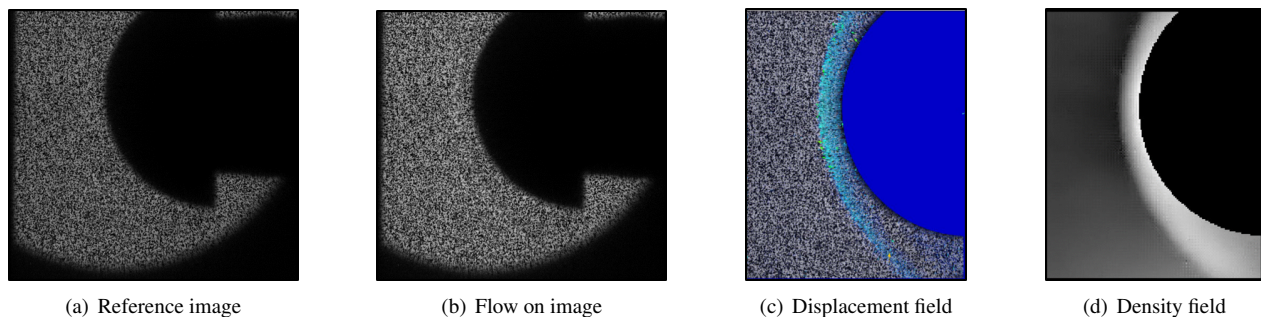


Figure 7: BOS measurement process

The nose-tip density increase rate due to the normal shock was measured for calibration and shock stand-off distance with the hemisphere model. Shock stand-off distance¹⁵ is an important parameter to assess flow quality in a shock tunnel. In many cases, because high pressure and temperature are maintained in the reservoir and a strong expansion along the hypersonic nozzle, the nozzle exit flow can induce a certain degree of thermo-chemical non-equilibrium or even freezes. Experimental results using the hemispherical model were compared with theoretical data established by Serbin³⁶ and reference data from Liepmann and Roshko.¹³ As a result, it was confirmed that the errors were 7.43% and 0.13%, respectively. The BOS measurement result of the density increase rate before and after the normal shock formed at the Mach number 6 flow condition was confirmed to be 5.23. It was confirmed that this has an error of about 0.8% when compared with the compressible flow theoretical value of 5.27(Fig.8(a)).

The validation of the density field measurement on the line from the center line of the test model to the oblique shock wave was conducted through the two dimensional cylinder model. To provide a two dimensional flow field, a test model with the same width as the nozzle exit diameter of 90 mm was used. Experimental and CFD visualization results are shown in Fig.8(b), and the flow characteristics including the recirculating region and recompression shock wave formed at the end of the model were qualitatively confirmed. Quantitative density measurement validation was conducted by comparing the results of BOS measurement with CFD at a position 6 mm from the rear end of the test

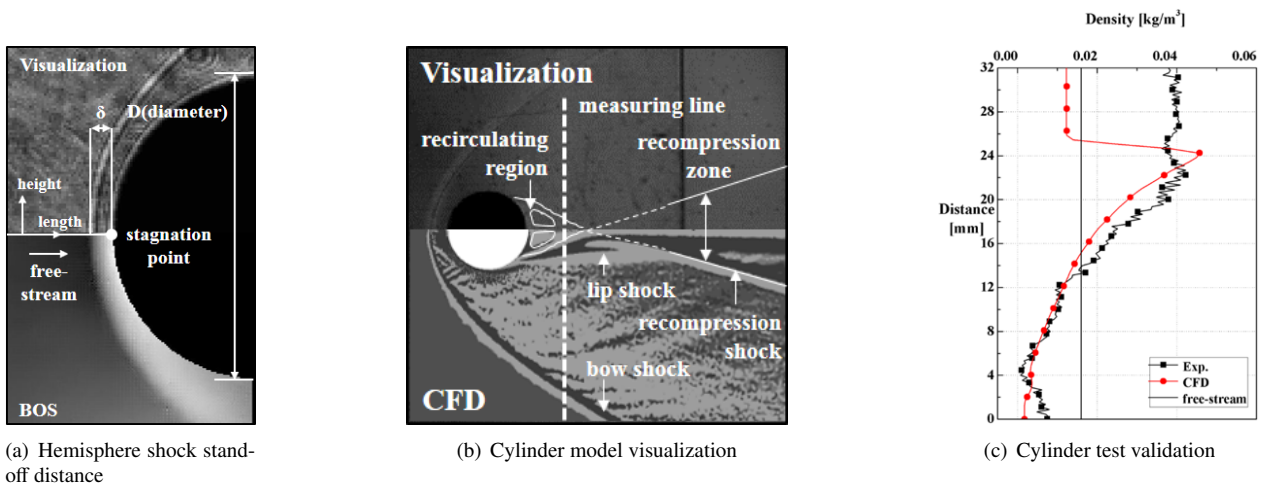


Figure 8: Density measurement validations

model. The cylinder model has a difference of about 7.3% at the peak point which is understood as the influence of the oblique shock wave, and it was confirmed that the density rising trend is well matched (Fig.8(c)). In the case of the cylinder model, beyond the oblique shock wave zone where the free-stream flows, computational results show that the density drops and the free-stream flow density value was recovered. However, it was confirmed that the experimental results have relatively high density values without density drop. This was caused by the size limitation of the shock tunnel nozzle-exit with 90 mm diameter. The density of the free-stream flow beyond the oblique shock wave at about 24.7 mm due to the narrow core flow zone was not recovered and was found to have a high density value of about 0.04 kg/m^3 .

4.2 Retro-jet experiment

Pressure calibration was carried out to confirm the chamber pressure 10 bar of the retro-jet single plume test model. The calibration was conducted in the order of 0.5, 1.0, 1.5, and 2.0 MPa, and the total pressure was measured to be 0.36, 0.83, 1.27, and 1.73 MPa, respectively. It was confirmed that the chamber pressure of 10 bar can be formed under the pressure of 1.19 MPa for the retro-jet single plume test model. The flow field formed by the interaction and interference between the retro-jet single plume and the opposing free-stream at the identified pressurized condition was determined by schlieren visualization. Fig.9(a) is the retro-jet single plume without the free-stream image, and Fig.9(b) shows the retro-jet plume with the free-stream image. Experimental visualization of high speed flow in the rarefied region was difficult to measure, but it was confirmed that the bow shock wave and the flow interface were stably formed in the steady state. The result of BOS measurement in the same retro-jet single plume experiment is shown in Fig.9(c). In this study, density field measurements were conducted at L1 position 12 mm apart from the retro-jet nozzle exit, L2 position 9 mm apart from the nozzle exit, L3 position 6 mm apart from the nozzle exit, L4 position 3 mm apart from the nozzle exit, and L5 position at the nozzle exit.

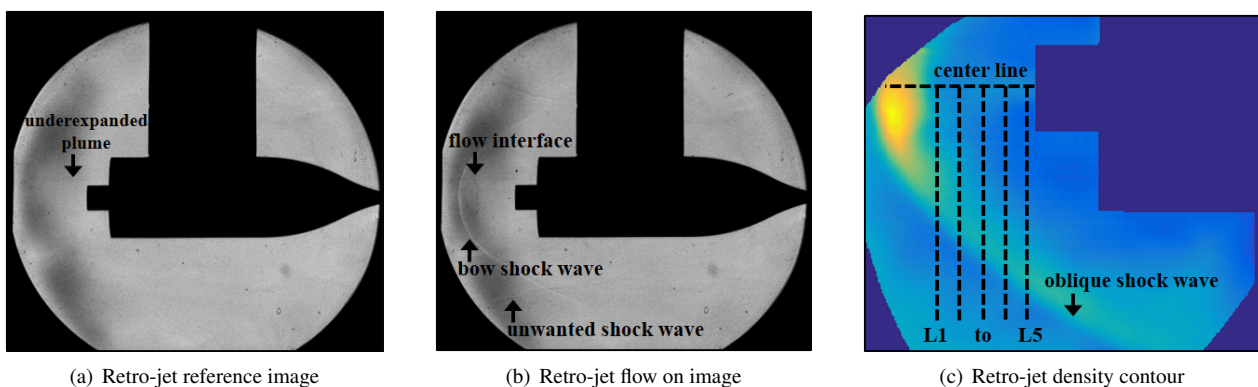


Figure 9: Retro-jet single plume test results

SHORT PAPER TITLE

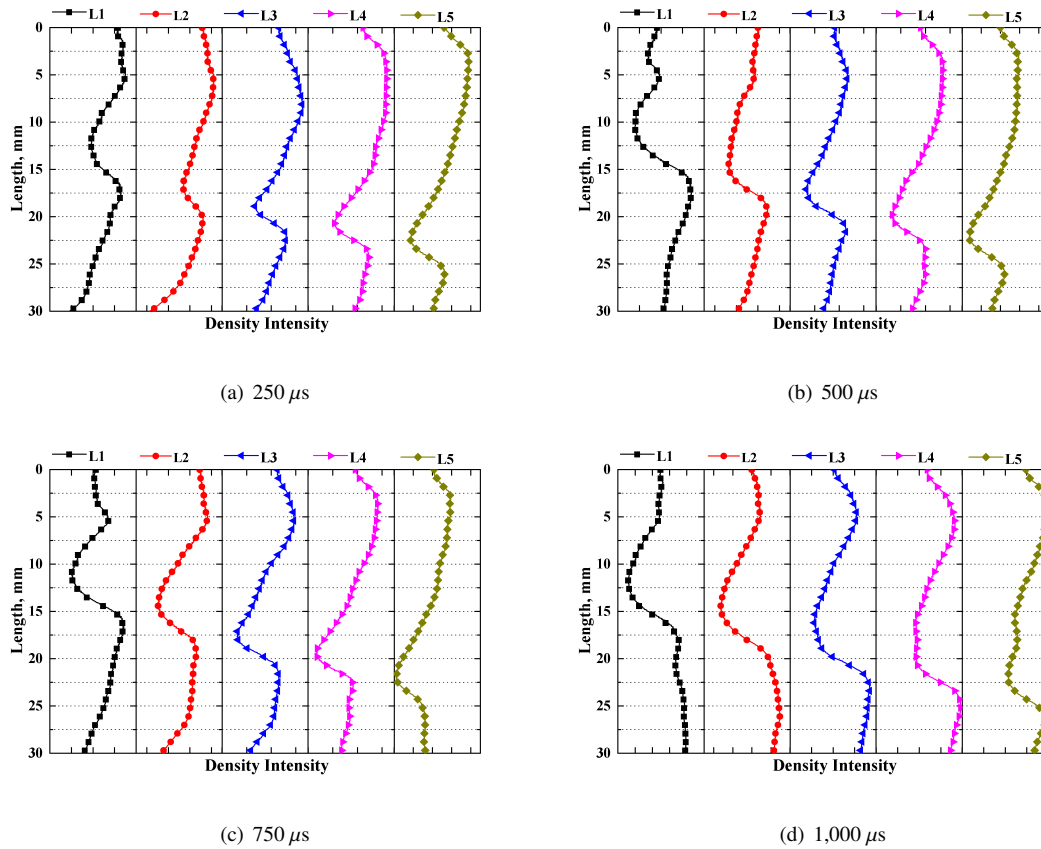


Figure 10: Density variation in each line that varies with time after flow reached

Flow fields were measured through four images in the steady state with $250 \mu\text{s}$ time intervals after the flow was arrived. A total of four images were measured due to the characteristics of the shock tunnel with an operation time of about 1 ms. The density changes in L1, L2, L3, L4, and L5 extracted from each image were measured as below (Fig.10). To identify and compare the retro-jet single plume thickness and oblique shock wave height, inflection points were confirmed where the tendency of density increases or decreases. Retro-jet single plume thickness was determined by inflection point at which density was decreased due to the high speed flow of the plume and then increased in density due to the recirculating region, and jet boundary and jet layer. The position of the oblique shock wave on the side of the retro-jet single plume was determined by confirming the inflection point at which the density, which was gradually increasing due to the recirculating region, jet boundary, jet layer, and flow interface, began to decrease. The positions of the retro-jet single plume thickness and oblique shock wave height extracted as below are summarized in Table3 and Table4. In the case of $250 \mu\text{s}$ after the free-stream reached(Fig.10), it was confirmed that the free-stream was in a steady state, but retro-jet single plume was not fully developed. The underexpanded retro-jet single plume was 3.15 mm, consistent with the steady state formed later in the nozzle exit (L5), but amplification of the plume thickness was observed at L3 line. As a result of the amplification, it was confirmed that the oblique shock wave height also increased in L2 and L3 lines by 16.0% and 11.3%, respectively, compared with the height in the steady state. Although the quantitative measurement of the flow field was not able to be confirmed in the images obtained by qualitative visualization(Fig.9(a),(b)), it was observed quantitatively whether the free-stream and the retro-jet single plume were sufficiently established by confirming the density inflection points(Fig.9(c)). Retro-jet single plume thicknesses were 5.01 ± 0.21 , 5.01 ± 0.21 , 4.77 ± 0.18 , 3.87 ± 0.31 , and 3.18 ± 0.14 from L1 to L5, respectively. The oblique shock wave heights were 11.16 ± 0.54 , 14.58 ± 0.31 , 16.98 ± 0.68 , 19.56 ± 0.21 , and 22.08 ± 0.21 from L1 to L5, respectively. The interaction between the retro-jet single plume and free-stream caused more longer duration to establish the stable flow field than without retro-jet single plume test.^{15,23}

In addition, the relationship between the position of the flow interface identified by the center line density trace, and the retro-jet nozzle thruster coefficient was confirmed. McGhee²⁷ investigated that increasing the nozzle-thrust coefficient C_T (Eq.7) in the steady-flow regimes results in a forward movement of the jet mach disk, flow-interface,

Table 3: Retro-jet single plume thickness comparison

	250 μ s	500 μ s	750 μ s	1,000 μ s
L1	5.13	5.13	5.13	4.77
L2	5.31	5.13	5.13	4.77
L3	8.37	4.95	4.77	4.59
L4	4.23	4.05	3.51	4.05
L5	3.15	3.33	3.15	3.06

dimensions are in millimeters

Table 4: Oblique shock wave height comparison

	250 μ s	500 μ s	750 μ s	1,000 μ s
L1	12.06	10.62	11.16	11.70
L2	16.92	14.76	14.22	14.76
L3	18.90	17.28	17.46	16.20
L4	20.70	19.80	19.44	19.44
L5	22.32	22.32	21.96	21.96

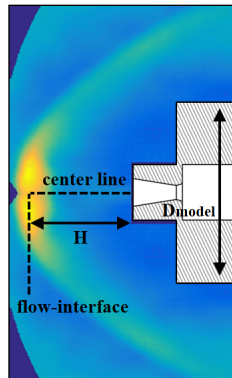
dimensions are in millimeters

and bow-shock locations. The jet mach disk location was largely dependent on C_T with little dependence upon free-stream Mach number. Both the flow-interface and bow-shock locations were also strongly influenced by C_T . It has been confirmed that H/D_{model} and C_T have values of 0.46 ± 0.008 and 0.30 in the steady state flow field, where H is the flow-interface distance, and D_{model} is the model base diameter. Compared with the literature results²⁷ with same M_∞ using a 114.3 mm test model with values of 0.48 and 0.30, respectively, it was confirmed that the flow-interface distance was not absolutely determined by the test model base diameter.

$$C_T = \frac{T}{q_\infty S} \quad (7)$$

$$T = \frac{\pi d_e^2}{4} (2q_j + p_j - p_\infty) \quad (8)$$

where T is the nozzle thrust(Eq.8), q_∞ is the dynamic pressure, S is the model base area, d_e is the nozzle exit diameter, q_∞ is the retro-jet dynamic pressure, p_j is the retro-jet static pressure, and p_∞ is the free-stream static pressure.



(a) Flow-interface position

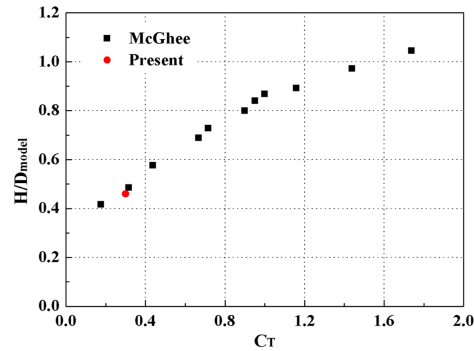
(b) Flow-interface location as a function of thrust coefficient (after McGhee²⁷)

Figure 11: Flow-interface location comparison

5. Conclusions

Experiments were carried out on general flow field features formed between retro-jet single plume and opposing free-stream. Qualitative measurements were conducted with schlieren photography, and measurements such as retro-jet single plume thickness and oblique shock wave height were measured quantitatively through an intrusive background oriented schlieren (BOS) technique. The BOS technique was verified by measuring the density increase rate before and after the bow shock wave and shock stand-off distance of the hemisphere model, and the density variation at the wake flow of the cylinder model. It was confirmed that retro-jet single plume thickness and oblique shock wave height can be measured quantitatively by applying the proved BOS measurement. In addition, retro-jet flow-interface distance and nozzle thrust coefficient were compared with literature.

6. Acknowledgments

This research was supported by Basic Science Research Program through the National Research Foundation of Korea (NRF) funded by the Ministry of Education(No.2018R1A6A3A01010886).

SHORT PAPER TITLE

References

- [1] The dc-x and dc-xa pages. https://www.hq.nasa.gov/office/pao/History/x-33/menu_dcx.htm. Accessed: 2019-06-17.
- [2] New shepard. <https://www.blueorigin.com/new-shepard/>. Accessed: 2019-06-17.
- [3] R. Beermann, L. Quentin, A. Pösch, E. Reithmeier, and M. Kästner. Background Oriented Schlieren Measurement of the Refractive Index Field of Air Induced by a Hot, Cylindrical Measurement Object. *Applied Optics*, 56(14):4168–4179, 2017.
- [4] S. A. Berry and M. N. Rhode. Supersonic retropropulsion test 1853 in nasa larc unitary plan wind tunnel test section 2. Technical Publication L-20392, NASA Langley Research Center, Apr. 2014.
- [5] S. A. Berry, M. N. Rhode, K. T. Edquist, and C. J. Player. Supersonic retropropulsion experimental results from the nasa langley unitary plan wind tunnel. In *42nd AIAA Thermophysics Conference*, pages 1–16. AIAA, Jun. 2011.
- [6] T. M. Cheung, F. F. J. Schrijer, and G. Park. Nitrogen Catalytic Recombination on Copper Oxide in Tertiary Gas Mixtures. *Journal of Spacecraft and Rockets*, 53(4):644–653, 2016.
- [7] U. Choi, J. Lee, H. Song, T. Sung, G. Park, and J. Ahn. A Study on Adaptive Design of Experiment for Sequential Free-fall Experiments in a Shock Tunnel. *Journal of the Korean Society for Aeronautical and Space Sciences*, 46(10):798–805, 2018.
- [8] M. Clem, C. Brown, and A. Fagan. Background Oriented Schlieren Implementation in a Jet-Surface Interaction Test. In *51st AIAA Aerospace Sciences Meeting including the New Horizons Forum and Aerospace Exposition*, pages 1–14. AIAA, Jan. 2013.
- [9] E. O. Daso, V. E. Pritchett, T.-S. Wang, D. K. Ota, I. M. Blankson, and Auslender A. H. The Dynamics of Shock Dispersion and Interactions in Supersonic Freestreams with Counterflowing Jets. *AIAA Journal*, 47(6):1313–1326, 2009.
- [10] T. Ecker, S. Karl, E. Dumont, S. Stappert, and D. Krause. A numerical study on the thermal loads during a supersonic rocket retro-propulsion maneuver. In *53rd AIAA/SAE/ASEE Joint Propulsion Conference*, pages 1–20. AIAA, Jul. 2017.
- [11] G. E. Elsinga, B. W. van Oudheusden, F. Scarano, and D. W. Watt. Assessment and Application of Quantitative Schlieren Methods: Calibrated Color Schlieren and Background Oriented Schlieren. *Experiments in Fluids*, 36(2):309–325, 2004.
- [12] P. J. Finley. The Flow of a Jet from a Body Opposing a Supersonic Free stream. *Journal of Fluid and Mechanics*, 26(2):337–368, 1966.
- [13] H. W. Liepmann, and A. Roshko. *Elements of Gas Dynamics*. John Wiley and Sons Inc., New York, 1957.
- [14] S. M. Jo, H. Shim, G. Park, O. J. Kwon, and J. G. Kim. Temperature Determination in a Shock Tube Using Hydroxyl Radical A-X Band Emission. *Physics of Fluids*, 31(2):026109, 2019.
- [15] I. Kim, S. Lee, G. Park, and J. K. Lee. Overview of Flow Diagnosis in a Shock Tunnel. *International Journal Aeronautical and Space Sciences*, 18(3):425–435, 2017.
- [16] I. Kim and G. Park. Experimental Study of Oxygen Catalytic Recombination on a Smooth Surface in a Shock Tube. *Applied Thermal Engineering*, In press, 2019.
- [17] I. Kim, G. Park, and J. J. Na. Experimental Study of Surface Roughness Effect on Oxygen Catalytic Recombination. *International Journal of Heat and Mass Transfer*, 138:916–922, 2019.
- [18] A. M. Korzun. Aerodynamic and performance characterization of supersonic retropropulsion for application to planetary entry and descent. PhD Thesis, Georgia Institute of Technology, 2012.
- [19] L. Venkatakrishnan, and G. E. A. Meier. Density measurements using the Background Oriented Schlieren technique. *Experiments in Fluids*, 37(2):237–247, 2004.

- [20] S. Lee. Aerodynamic characteristic study of space launch vehicle in ground tests. PhD Thesis, Korea Advanced Institute of Science and Technology, 2018.
- [21] S. Lee, B.-S. Oh, Y. Kim, and G. Park. A High-altitude Environment Simulation of Space Launch Vehicle in a Ground-test Facility. *Journal of the Korean Society for Aeronautical and Space Sciences*, 45(11):914–921, 2017.
- [22] S. Lee, B.-S. Oh, Y. Kim, and G. Park. High-altitude Environment Simulation of Space Launch Vehicle Including a Thruster Module. *Journal of the Korean Society for Aeronautical and Space Sciences*, 46(10):791–797, 2018.
- [23] S. Lee, H. Song, G. Park, and J. K. Lee. Freefalling Heated Sphere in a Shock Tunnel. *AIAA Journal*, 55(11):3995–3998, 2017.
- [24] M. Harker, and P. O’Leary. Least squares surface reconstruction from measured gradient fields. In *2008 IEEE Conference on Computer Vision and Pattern Recognition*, pages 1–7. IEEE, Jun. 2008.
- [25] M. Harker, and P. O’Leary. Least squares surface reconstruction from gradients: Direct algebraic methods with spectral, Tikhonov, and constrained regularization. In *CVPR 2011*, pages 2529–2536. IEEE, Jun. 2011.
- [26] M. Harker, and P. O’Leary. Direct regularized surface reconstruction from gradients for Industrial Photometric Stereo. *Computers in Industry*, 64(9):1221–1228, 2013.
- [27] R. J. McGhee. Effects of retronozzle located at the apex of a 140° blunt cone at mach numbers of 3.00, 4.50, and 6.00. Technical Publication L-7312, NASA Langley Research Center, Jan. 1971.
- [28] G. E. A. Meier. Computerized Background-Oriented Schlieren. *Experiments in Fluids*, 33(1):181–187, 2002.
- [29] G. Park. Oxygen Catalytic Recombination on Copper Oxide in Tertiary Gas Mixtures. *Journal of Spacecraft and Rockets*, 50(3):540–555, 2013.
- [30] M. M. Ragab, F. M. Cheatwood, S. J. Hughes, and A. Lowry. Launch vehicle recovery and reuse. In *SPACE 2015 Conference and Exposition*, pages 1–10. AIAA, Sep. 2015.
- [31] S. Raghunath and T. Roesgen. Visualization of Supersonic Flows in Shock Tunnels, using the Background Oriented Schlieren Technique. In *10th AIAA Australian Aerospace Student Conference*, pages 1–8. AIAA, Dec. 2004.
- [32] D. Ramanah. Background oriented schlieren technique for flow visualisation in shock tunnels. MS Thesis, The University of Queensland, 2007.
- [33] M. N. Rhode and W. L. Oberkampf. Estimation of uncertainties for a supersonic retro-propulsion model validation experiment in a wind tunnel. In *42nd AIAA Fluid Dynamics Conference and Exhibit*, pages 1–28. AIAA, Jun. 2012.
- [34] D. G. Schauerhamer, K. A. Trumble, B. Kleb, J.-R. Carlson, and K. T. Edquist. Continuing validation of computational fluid dynamics for supersonic retropropulsion. In *50th AIAA Aerospace Sciences Meeting including the New Horizons Forum and Aerospace Exposition*, pages 1–27. AIAA, Jan. 2012.
- [35] E. Seedhouse. *SpaceX’s Dragon: America’s Next Generations Spacecraft*. Springer Praxis books, London, 2016.
- [36] H. Serbin. Supersonic Flow Around Blunt Bodies. *Journal of the Aerospace Sciences*, 25(1):58–59, 1958.
- [37] H. Song, S. Lee, J. K. Lee, and G. Park. Attitude Angle and Drag Coefficient Measurements of Free-falling Hemisphere Using a Visualization Technique. *Journal of the Korean Society for Aeronautical and Space Sciences*, 45(8):619–626, 2017.
- [38] F. Sourgen, F. Leopold, and D. Klatt. Reconstruction of the Density Field using the Colored Background Oriented Schlieren Technique(CBOS). *Optics and Lasers in Engineering*, 50(1):29–38, 2012.
- [39] S. Stappert, J. Wilken, M. Sippel, and I. Dietlein. Evaluation of european reusable vtol booster stages. In *2018 AIAA Space and Astronautics Forum and Exposition*, pages 1–16. AIAA, Sep. 2018.
- [40] H. Takahashi, S. Tomioka, N. Sakuranaka, T. Tomita, K. Kuwamori, and G. Masuya. Influence of External Flow on Plume Physics of Clustered Linear Aerospikes Nozzles. *Journal of Propulsion and Power*, 30(5):1199–1212, 2014.

SHORT PAPER TITLE

- [41] H. Takahashi, S. Tomioka, T. Tomita, and N. Sakuranaka. Aerodynamic Characterization of Linear Aerospike Nozzles in Off-Design Flight Conditions. *Journal of Propulsion and Power*, 31(1):204–218, 2015.
- [42] L. Tian, S. Yi, Y. Zhao, L. He, and Z. Chen. Aero-Optical Wavefront Measurement Technique based on BOS and its Applications. *Chinese Science Bulletin*, 56(22):2320–2326, 2011.
- [43] L. Venkatakrishnan. Density Measurements in an Axisymmetric Underexpanded Jet by Background-Oriented Schlieren Technique. *AIAA Journal*, 43(7):1574–1579, 2005.
- [44] Y. Zhao, S. Yi, L. Tian, L. He, and Z. Cheng. An Experimental Study of Aero-Optical Aberration and Dithering of Supersonic Mixing Layer via BOS. *Science China Physics, Mechanics and Astronomy*, 53(1):81–94, 2010.
- [45] F. Zilker. Aerothermal analysis of re-usable first stage during rocket retro-propulsion. MS Thesis, Universität Stuttgart, 2018.